BILINGUAL PUBLISHING CO.
Pioneer of Global Academics Since 1984

02

Journal of Mechanical Engineering Research

Volume 3 | Issue 2 | September 2020 | ISSN 2630-4945 (Online)

Editor-in-Chief

Dr. Shankar Chakraborty

Jadavpur university, India

Editorial Board Members

Volume 3 Issue 2 • September 2020 • ISSN 2630-4945 (Online)

Journal of Mechanical Engineering Research

BILINGUAL PUBLISHING CO.

Pioneer of Global Academics Since 1984

BILINGUAL PUBLISHING CO.
Pioneer of Global Academics Since 1984

Volume 3 | Issue 2 | September 2020 | Page 1-23
Journal of Mechanical Engineering Research

Contents

Article

Review

BILINGUAL PUBLISHING CO.
Pioneer of Global Academics Since 1984

Journal of Mechanical Engineering Research
http://ojs.bilpublishing.com/index.php/jmer

ARTICLE

The Simulation on Dynamic of Rotary Inertia and Engine's Inflamer in Light Vehicle

Run Xu*

Gyeongsang National University, Metallurgical Engineering Department, Gyeongsang nam-do, Chinju, 52828, Korea

ARTICLE INFO

Article history
Received: 26 March 2020
Accepted: 15 April 2020
Published Online: 30 April 2020

Keywords:
Simulation
Dynamic
Car
Rotary inertia
Centripetal & circular acceleration
Driven force
Torque
Consumed fuel
Engine's inflamer

ABSTRACT

According to formula we can simulate their driven force and acceleration. The mechanical formula is used to obtain dynamics is used to simulate. The driven force increases when torque increases and tire diameter decreases. We need torque to increase so this is our plan. Acceleration raises when torque raises and it reduces when its weight raises. With the decreasing of radius of road the centripetal acceleration is increasing in the condition of light vehicle. It is that it decreases sluggishly before 0.35m/s2 then it maintains a steep decline to 0.62m/s2 and at last becomes sluggish again. It is valued that the economical efficiency about consumed fuel under different power. In the time of 0.2hr the fuel inflamer inclines sharply first then turns stable. It is the smallest value. Beyond it the fuel maintains a high value all the time. The discharged pollution gas decreases with the decreasing initial temperature. The low initial temperature is good to fuel gas. Meantime the smallest incline range is 300~350K which explains that it is the most save one.

1. Introduction

The power transmission of an vehicle is driven by torque, which is generated by the engine.Therefore, the measurement of torque is the evaluation of the vehicle power system, has an important role.[1,2] this paper studies the overall performance of the vehicle, including whether the braking performance of the vehicle achieves the best performance, through the torque, power and revolution of the vehicle engine.The kinematics of the vehicle takes speed and acceleration as research parameters and acceleration and braking as the main purpose of design.Therefore, the organic combination of power and movement is the real purpose of evaluating the car. Audi's 3.0t engine has a maximum power of 333ps, while Mercedes-benz's A45 AMG has a 2.0t engine of 360ps.With the increase of horsepower, their dynamic analysis and kinematics become particularly important. Such as torque and acceleration analysis. The horsepower of a truck is the most important factor. It is the main condition that designers should expect in advance that they can finish the task without environmental contamination. The car's load and less inflamer is the embodiment of its design level ability. The acceleration of the car is the main performance of the

**Corresponding Author:*
Run Xu,
Gyeongsang National University, Metallurgical Engineering Department, Gyeongsang nam-do, Chinju, 52828, Korea;
Email: xurun1206@163.com

 DOI: https://doi.org/10.30564/jmer.v3i2.1774

car, the acceleration is directly reflected in its function. A good engine function will be achieved in a relatively short time. Therefore, this paper explores whether the data of vehicle design are feasible based on the high power and acceleration of the vehicle, and discusses the status of high power and high torque to meet the needs of future vehicle development. Meantime the engine's inflamer properties is also proposed. [3,4]

2. Calculation Results and Discussion

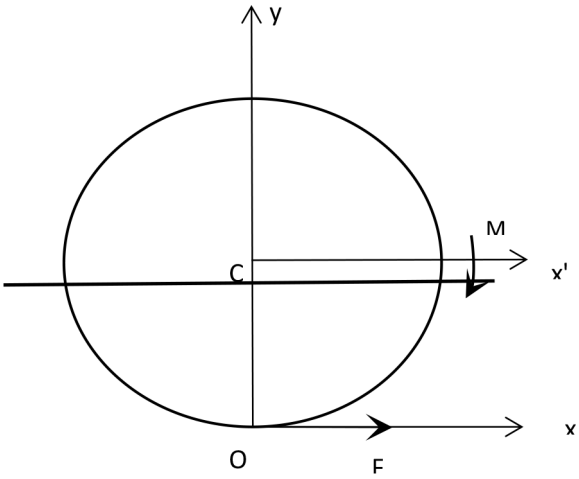

Figure 1. The relation of torque and Force on tire in car

Figure 1 shows the situation of vehicle tire subjected to torque and force.

From Newton's second law

$$F = ma \tag{1}$$

A is the tire acceleration, F is the force, and m is the mass.If C is the center of mass of the tire, R is the radius of the tire, and Mc is the torque of C.

2.1 Curve of Acceleration and Driving Force

2.1.1 Definition of Velocity

Because the moment of inertia of the wheel.

$$J_C = mR^2 / 2 \tag{2}$$

Here m is the mass of the car;A is acceleration.

In the reference frame with the center of mass at point C as the origin, the moment of motion of the particle system to point C refers to its moment of motion at this point in absolute motion

$$L_c = \sum M_c(m_i v_i) = \sum R_i * m_i v_i \tag{3}$$

If I take mi as the moving point x 'y' and z' as the moving point, I have

$$v_i = v_c + v_{i'} \tag{4}$$

Substitute into equation (3)

$$L_c = \sum m_i R_i^{'} * (v_c + v_{i'}) = \sum m_i R_i^{'} * v_c + \sum m_i R_i^{'} * v_{i'} \tag{5}$$

Due to the $\sum m_i R_i^{'} = \sum m_i R_c^{'} = 0$

So $L_c = \sum M_c(m_i v_{i'}) = \sum R_i^{'} * m_i v_{i'}$ (6).

The moment of force of a particle system on C is the same as the moment of force of a particle system calculated at its relative velocity or its absolute velocity.

And the same thing applies to the moment at fixed point O

$$L_o = \sum M_o(m_i v_i) = \sum R_i^{'} * m_i v_i \tag{7}$$

So the radius is R, and the absolute velocity is vi

The torque of the wheel at O

$$M_o = J_c \omega = mR^2 / 2 * \omega \tag{9}$$

2.1.2 Formula of Driving Force

The external force acting on the wheel can be simplified into plane force system F1, F2..., Fn uses the motion theorem of point C and the torque theorem of relative point C

$$ma = \sum F \tag{10}$$

Because angular acceleration $a = \frac{d\omega}{dt}$

$$\frac{d}{dt}(J_c \omega) = J_c \alpha = \sum M_c(F) \tag{11}$$

It can be converted into

$$m\frac{d^2 R}{dt^2} = \sum F \tag{12}.$$

And

$$J_c \frac{d^2 \varphi}{dt^2} = \sum M_c(F) \tag{13}$$

Because O is the origin of the original coordinate, and C is the origin of the new coordinate.

Let M be the moment, and let the moment of rotation be

DOI: https://doi.org/10.30564/jmer.v3i2.1774

$$M_c = M_0 - M_c^{'} \tag{14}$$

Since $M_0 = (mR^2/2)\cdot\alpha$ (15)

Parallel-motion coordinate system

$$M_c^{'} = FR \tag{16}$$

$$M_c = (mR^2/2)\cdot\alpha + FR \tag{17}$$

Because $a = R\alpha$ (18)

So $M_c = (mR^2/2)\cdot\alpha + FR$ (19)

Because $M_c^{'} = M$ (20)

So $M = FR + (mR^2/2)\cdot a/R$ (21)

Calculated and substitute below (31) to

$$a = 2M/3mR = \frac{2*9.554*P/n}{3mR} \tag{22}$$

Substitute (21) into the above equation to get

$$F = \frac{2M}{3R} = \frac{2*9.554*P/n}{3R} \tag{23}$$

2.1.2 Formula of Angular Acceleration

Figure 2 is the vehicle state of turn. R1is the radius of road; Mc is driven torque; Fc is centripetal force; R is the radius of tire.

The external force acting on the wheel can be simplified into plane force system F1, F2..., Fn uses the motion theorem of point C and the torque theorem of relative point C

$$ma = \sum F \tag{24}$$

Because angular acceleration $a = \frac{d\omega}{dt}$

$$\frac{d}{dt}(J_c\omega) = J_c\alpha = \sum M_c(F) \tag{25}$$

It can be converted into

$$m\frac{d^2R}{dt^2} = \sum F \tag{26}.$$

And

$$J_c\frac{d^2\varphi}{dt^2} = \sum M_c(F) \tag{27}$$

Because O is the origin of the original coordinate, and C is the origin of the new coordinate.

Let M be the moment, and let the moment of rotation be

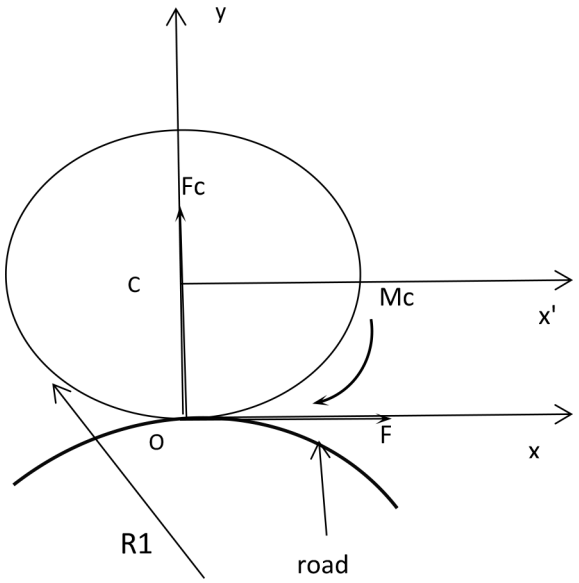

Figure 2. The vehicle state of turn. R1is the radius of road; Mc is driven torque; Fc is centripetal force; R is the radius of tire

$$M_c = M_0 - M_c^{'} \tag{28}$$

Since $M_0 = (mR^2/2)\cdot\alpha$ (29)

Parallel-motion coordinate system

$$M_c^{'} = FR \tag{30}$$

$$M_c = (mR^2/2)\cdot\alpha + FR \tag{31}$$

Because $a = R\alpha$ (32)

So $M_c = (mR^2/2)\cdot\alpha + FR$ (33)

Because $M_c^{'} = M$ (34)

So $M = FR + (mR^2/2)\cdot a/R$ (35)

Calculated and substitute below (33) to

$$FR = M - (mR^2/2)\cdot a/R \text{ is } F = M/R - \frac{mRa}{2} \quad (36)$$

Because $F = Ma$ (37)

And $F = \frac{mv^2}{R_1} = ma_\tau$ (38)

Because $v = v_0 + at$ (39)

Substitute (38) to (39) is

$$F = \frac{m(v_0 + at)^2}{R_1} = ma \text{ (40) gains}$$

$$(v_0 + a_\tau t)^2 / a_\tau < R_1 \text{ (41) is}$$

$$a_\tau t^2 < R_1 \text{ is}$$

$$a_\tau < R_1 / t^2$$

$$a_\tau = 2M/3mR = \frac{2*9.554*P/n}{3mR} \quad (42)$$

Substitute (37) into the above equation to get

$$F = \frac{2M}{3R} = \frac{2*9.554*P/n}{3R} \quad (43)$$

3. Discussion

3.1 Vehicle Driving Force and Acceleration Dynamics

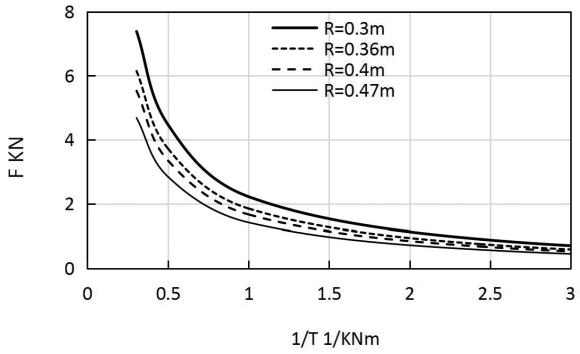

Figure 3. The relation of torque and force at 208KW of engine if R=0.3~0.4m in car

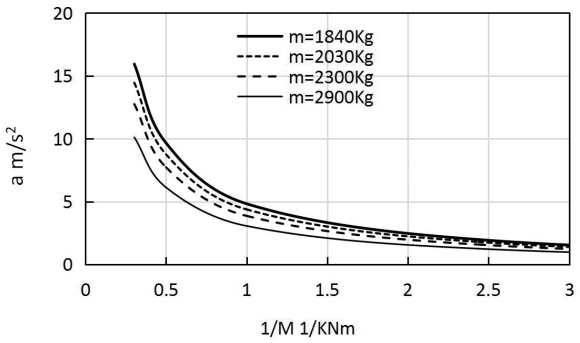

Figure 4. The relation of acceleration and torque if mass=1840~2900Kg in car under condition of 208KW

Figure 3 shows the curves of vehicle torque and force when tire radius R is 0.3~0.47 meters. At this time, the engine power is set at 208KW.As the tire diameter decreases the torque increases, so does the driving force.When the torque is 5KNm, the force reaches 10KN.

As shown in Figure 4 is curve of car acceleration a and torque M when the weight of car m=1840~290Kg and Power is 208KW, here use 208KW. When torque is 5KN-mthe acceleration is 5m/s^2. In Figure 4, when tire weight m=1840~290Kg, the curve between acceleration a and torque m of the car is selected as 208KW.As the mass of the car decreases and the acceleration increases, the torque increases and the acceleration increases, they are proportional.Therefore, when designing a car, it is necessary to choose lighter materials or reduce the amount of structure to reduce the weight, so as to increase the acceleration quickly.Increase speed in a very short time.

The curves of the torque and force of the car are shown in Figure 3. When the radius of the car tire is 0.3~0.4m, the forward force between the tire and the ground increases with the increase of the torque, and they form a straight line.The tire radius increases and the forward force decreases, which is why the torque constant force decreases. The difference between them is 2~3KN at 15KNm.Therefore, the tire radius should not be too large when designing a car.

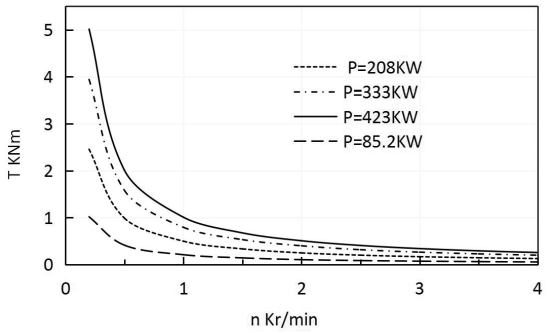

Figure 5. the relation of torque and rotary when P=85.2KW, 208KW, 333KW, 423KW in car

DOI: https://doi.org/10.30564/jmer.v3i2.1774

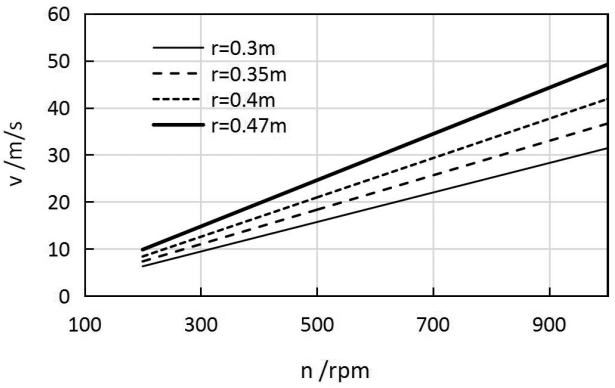

Figure 6. The relation of v and n in vehicle. N is the velocity. R is tire radius

Figure 5 shows the relationship between torque and power of an vehicle and the number of revolutions.The greater the power, the greater the torque.When the power P= 85.2kw ~423KW is 333KW, the torque increases to about 8KNm when the number of revolutions is less than 500rpm.As the number of revolutions increases, the torque decreases, and it remains at 2-3knm under various power conditions above 2000rpm.This means that the faster the car goes, the lower and closer the torque will be to the limit.When the power is 423KW and the speed is lower than 500r/min, the torque reaches 20KNm.When the power is 85.2kw, the torque reaches 4KNm.Considering the passenger or cargo capacity need not be too low, if 1-5 people in the car, there are some goods, then add 100-275kg of power. Figure 6 shows that v will increase when n increases in proportion. Meantime v will decrease when the R increases.

3.2 Vehicle Driving Force and Acceleration Dynamics

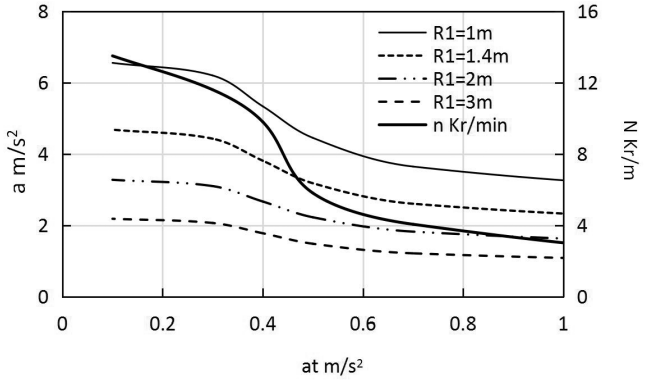

Figure 7. the relation of centripetal and circular acceleration in vehicle under condition of 85.4KW. N is the velocity. R1 is radius of load.

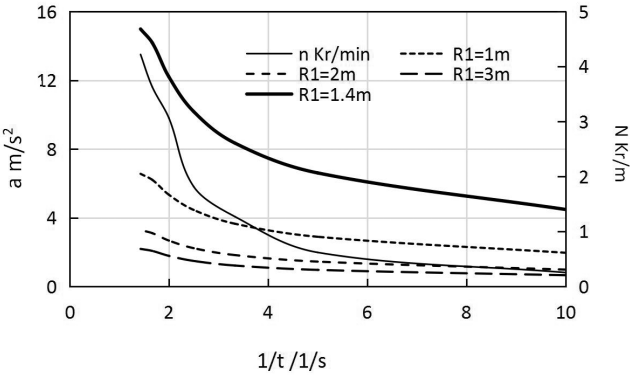

Figure 8. The relation of centripetal acceleration and 1/t in vehicle under condition of 85.4KW. N is the velocity. R1 is radius of load

As shown in Figure 7 the rpm is n and it is be left Y-axis ie.vertical coordinate the right axis is at circular acceleration while x-axis is centripetal acceleration. with the increasing of radius of road the at is decreasing in the condition of 85.4KW and 1.84ton of vehicle. Meantime with the increasing circular acceleration at the centripetal acceleration a is decreasing sluggishly before 0.35m/s^2 then it maintains a steep decline to 0.62m/s^2 and then becomes sluggish again. With the increasing of acceleration a the rpm is decreasing. It is due to inverse relation between n and a in terms of formula (42). The inverse relation of at and a is needed to study further to clarify the phenomenon. Why are they a parabola with increasing function there are negative curve here? We anticipate that the further investigation to do for it. As shown in Figure 8 the relation of acceleration and inverse time has been curved. The a will decrease with inverse time increasing. At the 41/s the at will be steep low and then it becomes softly low. With the increasing road curve radius from 1m to 5m a will decrease meantime. It fits to formula well. For the sake of improving a the small radius will be available and better. The relation of n and 1/t shows in here with the blue curve.

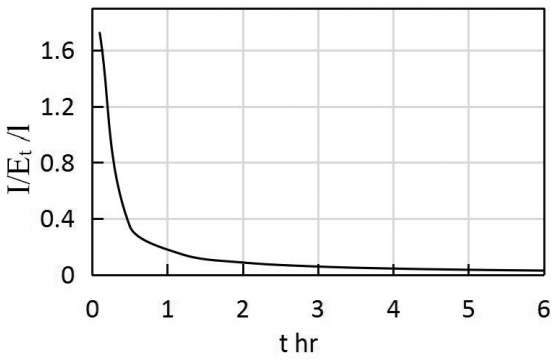

Figure 9. The relation of consumed fuel and time(hr) in engine of vehicle

 DOI: https://doi.org/10.30564/jmer.v3i2.1774

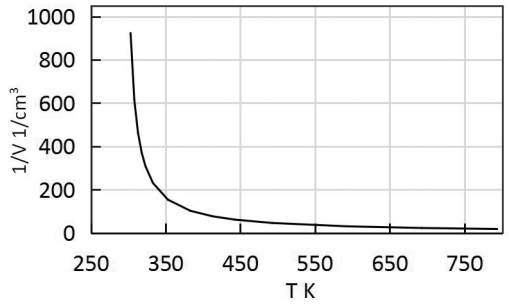

Figure 10. The relation of discharged pollution gas and temperature (K) in engine of vehicle

In Figure 9 it is observed that the consumed fuel $1/E_t$ is inverse proportional to time with the constant of 5.8l/100Km. When the time is 0.1 to 0.9 hours the $1/E_t$ is 59 ie. the consumed Fuel is from 0.016 to 0.125 liter respectively. In the time of 0.2 hr the curve gently declines. It indicates that the fuel inclines sharply first then turns stably. In Figure 10 it is found that the discharged pollution gas increases with the increasing initial temperature. Meantime the big steep range is 300~350K ie. 27~77℃. this explains that the steep rate of them is low.

4. Conclusion

(1) The greater the power, the greater the torque. As the number of revolutions increases, the torque decreases, and it remains at 2-3KNm under various power above 2000rpm. When the torque is 5KNm, the force reaches 10KN. As the mass of the car decreases and the acceleration increases, so does the torque and the acceleration. This is a destination for us to improve car properties. Therefore, when designing a car, it is necessary to choose lighter materials or reduce the amount of structure due to its weight so as to increase the acceleration quickly.

(2) With the increasing circular acceleration the centripetal acceleration is decreasing sluggishly before 0.35m/s^2 then it maintains a steep decline to 0.62m/s^2 and then becomes sluggish again. With the increasing of acceleration the rpm is decreasing. It is due to inverse relation between rotation and acceleration.

(3) In the time of 0.2 hr the curve gently declines. It indicates that the fuel inclines sharply first then turns stable. The discharged pollution gas increases with the increasing initial temperature. Meantime the big steep range is 300~350K ie. 27~77℃. this explains that the steep rate of them is low.

References

[1] Lianggui Pu, Guoding Chen, Liyan Wu. Mechanical Design[M]. Advanced Education Publisher, 2015, 24: 30.

[2] Shijie Fang, Yaoguang Qi. Mechanical Optimization Design[M]. Machinery Industry Publisher, 2003, 11.

[3] W S Peng, Z M Li, H l Huang. Mechanical Design[M]. Advanced Education Publisher, 2008: 195-196. (in Chinese)

[4] L Xu. Numerical prediction and support system of safety service life of remanufactured impeller considering damage fuzziness[D]. Chongqing University, 2017.

DOI: https://doi.org/10.30564/jmer.v3i2.1774

BILINGUAL PUBLISHING CO.
Pioneer of Global Academics Since 1984

Journal of Mechanical Engineering Research
http://ojs.bilpublishing.com/index.php/jmer

ARTICLE

The Dynamic Simulation of Rotary Inertia on Light vehicle-Slope I

Run Xu* Boyong Hur

Gyeongsang National University, Metallurgical Engineering Department, Gyeongsang nam-do, Chinju, 52828, Korea

ARTICLE INFO

Article history
Received: 13 April 2020
Accepted: 22 April 2020
Published Online: 30 April 2020

Keywords:
Simulation
Dynamic
Light vehicle
Acceleration
Turn bending
Driven force
Torque
Rotation
Slope

ABSTRACT

According to formula we can simulate their driven force and acceleration on the slope. The mechanical formula is used to obtain force and theoretical dynamics in the slope. The driven force decreases when rotation increases. When power increases the acceleration increases. it reduces when its weight raises. It is found that the a will decrease as slope becomes high from 5 to 11° to 22°, which fit the formula too. Meantime as the radius is high from 0.3m to 0.4m to 0.47m a will be low. The needed force will increase as the slope decline becomes big at the same power.

1. Introduction

The power transmission of an light vehicle is driven by power on the gradient, which is generated by the engine. Therefore, the measurement of power is the evaluation of the light vehicle engine system on the gradient, has an important role [1,2,3]. This paper studies the overall performance of the light vehicle, including whether the gradient performance of the light vehicle achieves the best performance, through the power and revolution of the light vehicle engine. The kinematics of the light vehicle takes speed and acceleration as research parameters and acceleration as the main purpose of design. Therefore, the organic combination of power and movement is the real purpose of evaluating the light vehicle. Audi's 3.0t Engine has a maximum power of 333hp, while Mercedes-benz's A45 AMG has a 2.0t engine of 360hp. With the increase of horsepower, their dynamic analysis and kinematics become particularly important. Such as force, acceleration and rotation analysis.The horsepower of a truck is the most important factor. It is the main condition that designers should expect in advance that they can finish the task without failure.The light vehicle's load and acceleration etc. less trouble is the embodiment of its design level ability. The acceleration of the light vehicle is the main performance of the light vehicle, the force and acceleration is directly reflected in its engine function. A good engine function will be achieved in a relatively short

**Corresponding Author:*
Run Xu,
Gyeongsang National University, Metallurgical Engineering Department, Gyeongsang nam-do, Chinju, 52828, Korea;
Email: xurun1206@163.com

 DOI: https://doi.org/10.30564/jmer.v3i2.1800

time in a slope. Therefore, this paper explores whether the data of light vehicle design are feasible based on the high power and acceleration of the light vehicle on here, and discusses the status of high power and high acceleration to meet the needs of future light vehicle development on a slope.

2. Calculation Results

As shown in Figure 1 it is a vehicle driving forwards along the slope with θ. Here a is the tire acceleration, F is the force, and m is the mass. If *C* is the center of mass of the tire, R is the radius of the tire, and Mc is the torque of *C*. *O* is xy original point and *C* is x'y point.

If the vehicle runs at slope plane with θ, there is $md^2R/dt^2=\Sigma F$ and $J_c d^2\varphi/dt^2=\Sigma M_c$

$$F_s = m\sin\theta \tag{1}$$

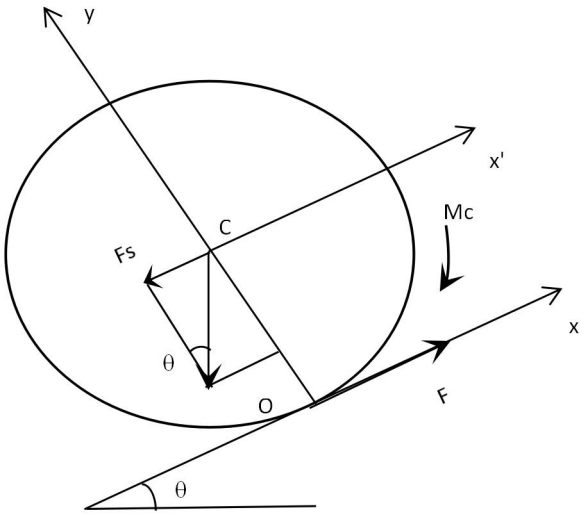

Figure 1. The relation of torque and Force on tire on the slope load in light vehicle, here q is slope angle

Referring to C $$\frac{a}{R}\cdot\frac{mR^2}{2}+F\cdot R=M_c \tag{2}$$

Referring to C $$M_c = F_s R \tag{3}$$

Substitute to below (4)

$$F - F_s = ma \tag{4}$$

Obtain

$$F=(M_c-\frac{mR^2}{2})/R=M_c/R-\frac{ma}{2} \tag{5}$$

Ie $$M_C=\frac{mR^2}{2}+FR \tag{6}$$

Due to $$F_s < F \tag{7}$$

Substitute (5) into (2)

$$a\frac{mR}{2}+(M_c/R-\frac{ma}{2})=M_c \tag{8}$$

Ie

$$a=\frac{2M_c(1-1/R)}{m(R-1)} \tag{9}$$

Or due to

$$F-F_s=ma \tag{10}$$

Is $$a=(F-F_s)/m=\frac{M}{Rm}-\frac{a}{2}-\sin\theta \tag{11}$$

Ie

$$a=\frac{2}{3}(\frac{M}{Rm}-\sin\theta) \tag{12}$$

and

$$F=M/R-\frac{ma}{2} \tag{13}$$

Prove too above equation.
Substitute (12) into above is

$$F=\frac{2M}{3R}+\frac{m}{3}\sin\theta \tag{14}$$

3. Discussion

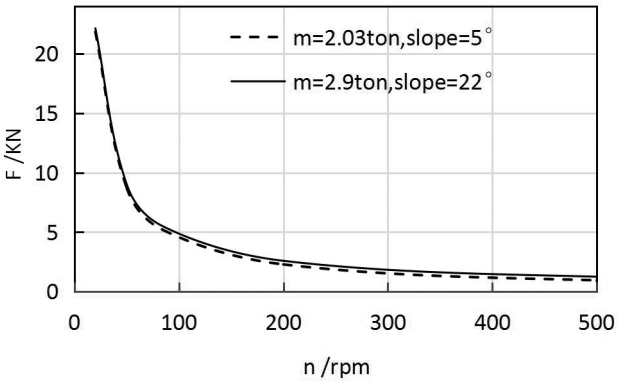

(a) r=0.5m

DOI: https://doi.org/10.30564/jmer.v3i2.1800

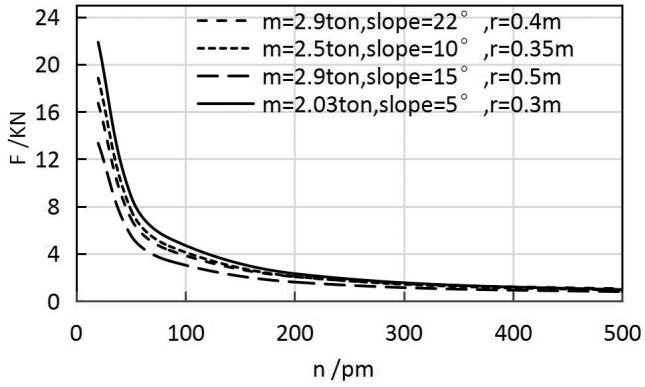

(b)

Figure 2. The relation force and rotation in light vehicle at the 85.2KW

Figure 2(a) shows the curves of light vehicle force and rotation when tire tire radius R is 0.5 meters. At this time, the engine power is set at 85.3KW. As the tire slope decreases into 5° the torque decreases some. meantime the force decreases with rotation ie. rotation increases the force decreases too. It fits to formula well. When the rotation is 100r/m, the force reaches 5KN steeply. Then the force changes to decrease sluggishly. At 400r/m it reaches 2r/m. As the tire radius r decreases into 0.3m the force will be higher than that into 0.4m. It fits to the formula well too. At rotation being 300r/m it will be constant at radius 0.3m & 0.4m. It is due to big θ resulting big force in terms of formula (14). Table 1 is the parameters in this study. There are mass、tire radius & powers respectively. When the slope is above 20° the high force is needed. It needs small radius、high power & heavy weight for the moment of inertia optimum design. Otherwise the cease fire will happen due to weak power.

As shown in Figure 3(a,b,c), when horsepower is 115~575 & tire mass is 2030~2890Kg, they are the curves between acceleration and rotation of the light vehicle. As horsepower increases the mass of the light vehicle increases the acceleration increases, they are inverse proportional. It is due to the big horsepower firstly then the mass little. Therefore, when designing a light vehicle, it is necessary to choose big power one and the light weight as possible, so as to increase the acceleration a very short time and save cost.

It is found that the a will decrease as slope becomes high from 5 to 11° to 22°, which fit the formula too. Meantime as the radius is high from 0.3m to 0.4m to 0.47m a will be low. So it is chosen that the small slope and use small tire radius is to promote acceleration in motion.

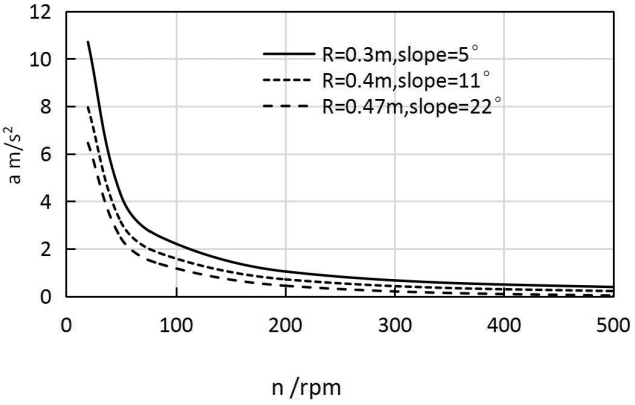

(a) 115 horses; 2.03tons

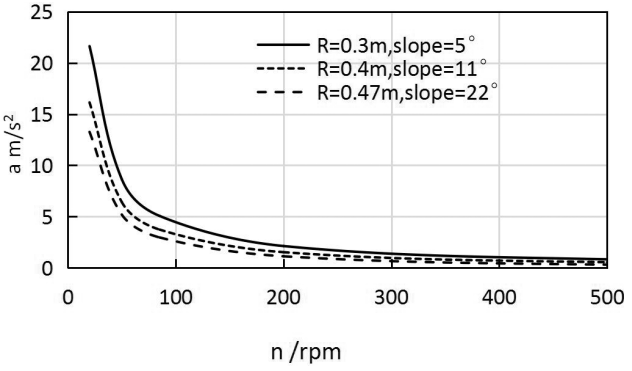

(b) 283 horses; 2.5tons

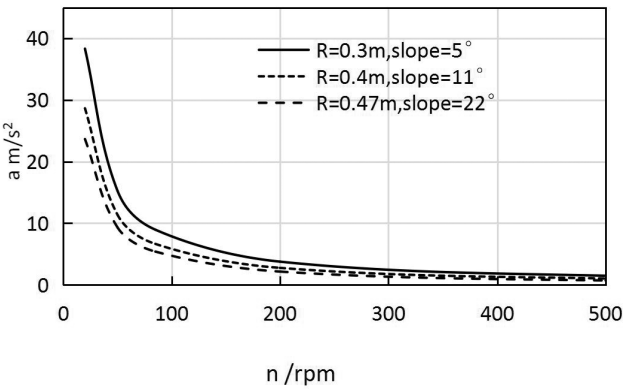

(c) 574 horses; 2.89tons

Figure 3. The relation of acceleration and torque in light vehicle if R=0.3, 0.4,0.47mm

Table 1. The mechanical parameters in light vehicle

No. \ Item	light vehicle mass /Kg	Tire radius /m	Engine power / KW
1	2030	0.30	85.3
2	2300	0.35	208
3	2900	0.47	423

 DOI: https://doi.org/10.30564/jmer.v3i2.1800

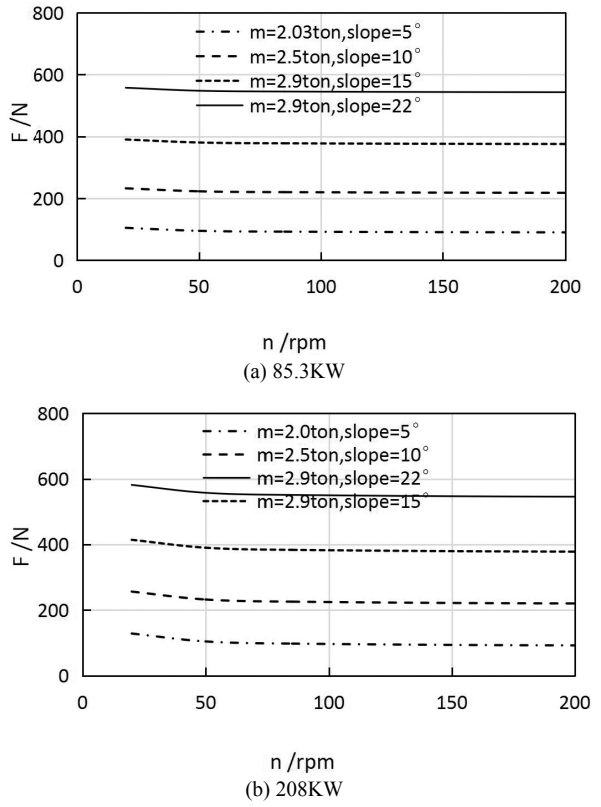

Figure 4. The relation of force and rotary in light vehicle at the 85.2KW and 208KW

The force will decrease a little when power is 208KW to compare with 85.3KW from Figure 4 (a,b). It expresses that the a little more force is produced in high power as the value is near neglectful. In addition the little decrease happens too below 50r/m due to relatively high velocity. Meantime the force will maintain a about constant after this point with a sluggish decline. This is since the low torque caused by high rotary and slope angle increases which results in some drag down. These two factors interact together to offset force. This is a main reason to be found sluggish force decrease here in this paper. The needed force will increase as the slope decline becomes big at the same power.

4. Conclusions

(1) According to formula we can simulate their driven force and acceleration on the slope. The mechanical formula is used to obtain force and theoretical dynamics in the slope. The driven force decreases when rotation increases. When power increases the acceleration increases. it reduces when its weight raises.

(2) It is found that the a will decrease as slope becomes high from 5 to 11° to 22°, which fit the formula too. Meantime as the radius is high from 0.3m to 0.4m to 0.47m a will be low. The needed force will increase as the slope decline becomes big at the same power.

References

[1] Lianggui Pu, Guoding Chen, Liyan Wu. Mechanical Design[M]. Advanced Education Publisher, 2015, 24: 30.

[2] Shijie Fang, Yaoguang Qi. Mechanical Optimization Design[M]. Machinery Industry Publisher, 2003: 11.

[3] W S Peng, Z M Li, H l Huang. Mechanical Design[M]. Advanced Education Publisher, 2008: 195-196.

DOI: https://doi.org/10.30564/jmer.v3i2.1800

BILINGUAL PUBLISHING CO.
Pioneer of Global Academics Since 1984

Journal of Mechanical Engineering Research
http://ojs.bilpublishing.com/index.php/jmer

ARTICLE

Optimal Batching Plan of Deoxidation Alloying based on Principal Component Analysis and Linear Programming

Zinan Zhao* Shijie Li Shuaikang Li

Metal Materials Engineering, Metallurgy and Energy College of North China University of Science and Technology, Tangshan, Hebei, 063210, China

ARTICLE INFO

Article history
Received: 21 May 2020
Accepted: 21 May 2020
Published Online: 31 May 2020

Keywords:
Deoxidization alloying
Principal component regression analysis
Linear programming
Optimization of dosing scheme

ABSTRACT

As the market competition of steel mills is severe, deoxidization alloying is an important link in the metallurgical process. To solve this problem, principal component regression analysis is adopted to reduce the dimension of influencing factors, and a reasonable and reliable prediction model of element yield is established. Based on the constraint conditions such as target cost function constraint, yield constraint and non-negative constraint, linear programming is adopted to design the lowest cost batting scheme that meets the national standards and production requirements. The research results provide a reliable optimization model for the deoxidization and alloying process of steel mills, which is of positive significance for improving the market competitiveness of steel mills, reducing waste discharge and protecting the environment.

1. Introduction

The deoxidation alloying in the steelmaking process is an important process in steel smelting. Deoxidation alloying means that for different steel types, different amounts and different types of alloys need to be added at the end of smelting to remove oxygen elements as much as possible to make the alloy elements contained meet the standards, and finally make the finished steel have certain physical properties to meet specific requirements.

The deoxidation alloying of molten steel mainly concerns the content of five elements of C, Mn, S, P, and Si. As basic alloying elements, C, Mn and Si play the role of solid solution strengthening, which significantly improves the strength and hardness of the steel and improves the hardenability of the steel. Thus the content needs to be controlled. The presence of P and S in the steel will harm the safe use of the steel. The phenomenon of cold brittleness and hot brittleness will appear, reducing the plastic toughness of the steel. The content needs to be strictly controlled.

The general research direction is to establish a mathematical model for the deoxidation alloying link through historical data, online prediction and optimization of the type and quantity of the alloy input, while ensuring the quality of the molten steel and minimizing the production cost of alloy steel.

Scholars have done a lot of research on the deoxidization and alloying of molten steel. Hu Jingtao established the LF deoxidization and alloying model, studied the

**Corresponding Author:*
Zinan Zhao,
Metal Materials Engineering, Metallurgy and Energy College of North China University of Science and Technology, No. 21 Bohai Avenue, Tangshan Bay Ecological City, Caofeidian, Tangshan, Hebei, 063210, China;
Email: 2562275375@qq.com

 DOI: https://doi.org/10.30564/jmer.v3i2.1903

feeding amount of aluminum wire in molten steel, and established the minimum cost model by simplex method and considering the price factor [1]; Chunxia Zhang used the artificial neural network BP model to deal with the yield parameters of alloy elements, and used the multiple linear programming method to calculate the optimal ingredients of alloying operation, and obtained the engineering results A practical control model for deoxidization and alloying [2]. However, BP neural network algorithm requires a large amount of data, and will inevitably appear "zigzag phenomenon", which makes BP algorithm inefficient. Zhe Xu used the fuzzy modeling method to study the prediction method of the recovery rate of molten steel alloy elements and the optimization of ingredients in the ladle refining process [3]; Wenle Zhang studied the particle swarm optimization algorithm and simulated annealing algorithm for the LF refining furnace alloying, and analyzed the main factors affecting the recovery rate of alloy in the ladle refining process [4], and the convergence speed of simulated annealing algorithm The performance of the algorithm is related to the initial value and parameter sensitivity. Ruonan Cheng, et al. Used Pearson correlation coefficient to get the relationship between different factors and element yield, established BP neural network model optimized by multiple linear programming to predict the yield of C and Mn, and analyzed the optimal proportioning scheme with SPSS [5]. However, Pearson correlation coefficient method does not consider the impact of the number of overlapping records on the similarity. Yu Dai, et al. Obtained the main factors that affect the rate of C and Mn by using the grey correlation model. On this basis, the multi-objective optimization model with the lowest price and the lowest element content error was established for the burden problem. So we can get the best proportioning scheme [6]. However, the subjectivity of grey model is too strong, and the optimal value of each index needs to be determined currently. According to the formula of alloy yield, Huiling Zhou, et al. Obtained the historical yield of C and Mn elements, and established the model of influencing factors of yield based on factor analysis. Then, the multiple linear regression equations of C and Mn element yield and influencing factors are established, and finally the predicted values of C and Mn element yield are obtained [7]. Fangyu Liu, et al. Calculated the yield of C and Mn based on the data, screened out the main factors influencing the yield by Pearson correlation coefficient, obtained the prediction equation of the yield of C and Mn by multiple linear regression analysis, and then verified and improved the prediction model by BP neural network, finally realized the optimization of the cost of deoxidization and alloying of molten steel [8]. Pengmai Liu, et al established the BP neural network model for the prediction of the recovery rate of C and Mn elements, and further improved the model and algorithm to improve the prediction accuracy of the recovery rate of elements [9]. Combined with the research of scholars, based on the idea of mathematical model, a reliable prediction model and optimization model are designed for the recovery rate of elements and the proportioning scheme, so as to improve the utilization rate of raw materials in the deoxidization and alloying process and reduce the production cost.

2. Factors Affecting Yield

The yield of alloying elements is an important indicator to be concerned during the deoxidation alloying process. The element yield reflects the utilization rate of important alloying elements in the alloying batching scheme and reflects the feasibility of the scheme. Too low an element yield will cause waste of raw materials, reduce production efficiency, and cause environmental pollution. Studying the yield of alloying elements has a positive effect on establishing the deoxidation alloying batching scheme.

2.1 Principal Component Analysis

In production, there are many factors that affect the yield of the alloy, such as the end temperature of the converter, the net weight of the molten steel, and the addition of raw materials. For multi-factor high-dimensional problems, a mathematical model based on the principal component analysis method is established. Subsequent problems are solved by evaluating the contribution of the principal component and reducing the dimension.

Principal component analysis uses *p*-dimensional vectors $\vec{x} = \left(x_1, x_2, \cdots, x_p\right)$ false. Standardize the original indicator data $\overrightarrow{x_i} = \left(x_{i1}, x_{i2}, \ldots, x_{ip}\right)^T, i = 1, 2, \cdots, n$. Then construct the sample matrix.

$$M_{sample} = \begin{pmatrix} x_{11} & x_{12} & \cdots & x_{1p} \\ x_{21} & x_{22} & \cdots & x_{2p} \\ \vdots & \vdots & \vdots & \vdots \\ x_{n1} & x_{n2} & \cdots & x_{np} \end{pmatrix} \tag{1}$$

Standardized transformation of sample array elements.

$$Z_{ij} = \frac{x_{ij} - \overline{x_j}}{S_j}, i = 1, 2, \cdots, n; j = z, 2, \cdots, p \tag{2}$$

Through the above changes, a standardized matrix *Z* is

DOI: https://doi.org/10.30564/jmer.v3i2.1903

obtained. Then find the correlation coefficient matrix for the standardized matrix.

$$R=\left[r_{ij}\right]_p \quad xp=\frac{Z^T Z}{n-1},\ r_{ij}=\frac{\sum z_{kj}\cdot z_{kj}}{n-1}, i,j=1,2,\ldots,p \quad (3)$$

Solve the characteristic equation of the sample correlation matrix.

$$\sum_{j=1}^{m}\lambda_j \Big/ \sum_{j=1}^{p}\lambda_j \geq 0.85 \quad (4)$$

Determining the value of m can satisfy the information utilization rate of more than 85%. For each $\lambda_j\left(j=1,2,\cdots,m\right)$, Solve equations $R\vec{b}=\lambda_{jb}$, can get the unit feature vector $\overrightarrow{b_j^o}$. Convert standardized index variables to main components $U_{ij}=Z_i^T\overrightarrow{b_j^o}, j=1,2,\ldots,m$. Among them, U_1 is called the first principal component, U_2 is called the second principal component, and U_p is called the p-th principal component. Finally, comprehensive analysis and weighted sum of the m principal components are obtained to obtain the final evaluation value, and the weight is the variance contribution rate of each principal component. The principal component analysis of the factors affecting the yield of C and Mn alloys can be achieved.

2.2 Regression Analysis

Based on principal component analysis, a prediction model of alloy yield can be established. However, the accuracy of Principal component analysis prediction model is not high, and its accuracy is about 50%. In order to improve the accuracy of prediction, the principal component analysis model was optimized by means of multiple regression analysis [10].

In principal component analysis, the principal components, expressions and variables that satisfy the information contribution rate of more than 85% have been obtained.

$$U=W\vec{x} \quad (5)$$

At the same time, the alloy historical yield is transformed into a column vector and combined with the sample matrix into a new sample matrix. The principal component analysis is carried out on the new sample matrix, and the new characteristic roots and eigenvectors are obtained. The linear coefficients of each principal component can be obtained by multiple regression analysis of the corresponding eigenvectors and principal component matrices.

The yield of the alloy can be predicted according to the coefficient matrix when the independent variables (influencing factors) are given.

3. Optimize the Batching Plan

Based on the actual production requirements of cost and elements, new constraints can be added to the prediction model, and the method of linear programming can be adopted to make it more in line with the reality, and the mathematical model of cost optimization can be established.

3.1 Objective Function

The objective function is set to cost. The constraint conditions are set as yield constraint, element content constraint and non-negative quality constraint.

$$\omega=\sum_{a=1}^{16}\left(m_a\cdot s_a\right) \quad (6)$$

At the same time, Set the addition amount of various alloys. The cost of the alloy batching scheme is the product of the amount of raw materials added to the alloy and the unit price.The cost constraint is the requirement that the cost be as small as possible.

3.2 Yield Constraint

According to formula 4 and decision variable m_a, the yield prediction formula is

$$\chi=B\vec{x}=B\left(x_1,x_2,\cdots,x_9,m_1,m_2,\cdots,m_{16}\right)^T.$$

Where B represents the coefficient matrix. It should be pointed out, $x_1,x_2,\cdots,x_9$ indicate the nature of molten steel itself, which is set as a constant in the cost optimization model. $m_1,m_2,\cdots,m_{16}$ decision variable. The yield constraint requires the alloy yield to meet the basic requirements.

$$\chi\geq\left[\chi\right] \quad (7)$$

At the same time, the yield should be no more than 1.

$$\left[\chi\right]\leq\chi\leq 1 \quad (8)$$

3.3 Elemental Content Constraints

Different types of steel require that the content of each

 DOI: https://doi.org/10.30564/jmer.v3i2.1903

element must conform to the national standard, so the element content constraint condition is the requirement of the target composition of molten steel.

$$Bl_j \le \frac{\sum_{i=1}^{16} c_{a,j}\chi_j m_a + b_j P}{P+\Delta P} \le Bu_j \tag{9}$$

In the formula, j represents the element to be alloyed, $j=1,2,\cdots,m$; $c_{a,j}$ represents the content of j falseelement in the i-th alloy; χ_j represents the yield of element j. m_a represents the amount of alloy added; b_j falserepresents the content of element j in the original molten steel; P is the weight of the original molten steel (kg); ΔP represents the added weight of molten steel (kg); Bl_j represents the lower limit of the requirement of the j-th element in molten steel; Bu_j represents the upper limit of the requirement of the j-th element in molten steel [11].

3.4 Non-negative Constraints

The minimum alloy addition amount is 0, the addition amount below 0 has no practical significance and should not be considered here.

3.5 Linear Programming

In above constraints, ΔP in the inequality of the requirement for the target component of molten steel is related to the alloy addition amount ma, that is, the constraint condition is not a general form of linear programming problem. To use the improved simplex method, first need to use m_a to represent ΔP, and to reduce the constraints to the general form of the linear programming problem [12]. Assuming that all the alloys are put into molten steel, the linear constraints are obtained.

$$\sum_{a=1}^{n}\left(c_{aj}-\frac{Bu_j}{\chi_j}\right)m_a \le \frac{P\left(Bu_j-b_j\right)}{\chi_j} \le \sum_{a=1}^{n}\left(c_{aj}-\frac{Bl_j}{\chi_j}\right)m_a \tag{10}$$

After adding relaxation variables and residual variables and combining the cost constraint and non-negative condition formula, a general mathematical model for calculating the minimum cost alloy addition in the process of deoxyalloying can be obtained. The constraints are as follows.

$$\begin{cases} \sum_{a=1}^{n}\left(c_{a1}-\frac{Bu_{j1}}{\chi_1}\right)m_a + m_{n+1} = \frac{P\left(Bu_1-b_1\right)}{\chi_1} \\ \sum_{a=1}^{n}\left(c_{a1}-\frac{Bl_1}{\chi_1}\right)m_a - m_{n+2} = \frac{P\left(Bl_1-b_1\right)}{\chi_1} \\ \cdots \\ \sum_{a=1}^{n}\left(c_{am}-\frac{Bu_{jm}}{\chi_m}\right)m_a + m_{2m-1} = \frac{P\left(Bu_m-b_m\right)}{\chi_m} \\ \sum_{a=1}^{n}\left(c_{am}-\frac{Bl_{jm}}{\chi_m}\right)m_a - m_{2m} = \frac{P\left(Bl_m-b_m\right)}{\chi_m} \\ m_a \ge 0\left(a=1,2,\cdots,n;\ j=1,2,\cdots,m\right) \end{cases} \tag{11}$$

This model is suitable for the calculation of various elements in alloys. In the case that the alloy contains only one alloying element and this alloying element exists only in the alloy (such as aluminum), the addition amount of the alloy is not involved in the model calculation, and the formula can be directly applied.

$$Bl_j \le \frac{\chi_i m_a + b_j P}{P+\Delta P} \le Bu_j \tag{12}$$

4. Result Analysis

The data comes from the D question of the MathorCup Mathematical Modeling Competition 2019, including historical data of steelmaking and description of various alloy materials. In order to solve the problem, the following assumptions are proposed: it is assumed that the occurrence of abnormal data is due to the reaction of steel slag or the special effect of the deoxidizer; it is assumed that only the composition of the feed is optimized, and the influence of the addition of alloy ingredients on the furnace temperature and other factors is not considered; Assuming that the historical data of steelmaking and various alloy materials in the appendix are accurate. Through principal component regression analysis and linear analysis, the model of C and Mn alloy yield and optimization of the batching scheme can be obtained.

4.1 Principal Component Analysis

Using MATLAB, the main component analysis of the factors affecting the yield of C and Mn alloys was achieved. The results are shown in Table 1 and Table 2.

DOI: https://doi.org/10.30564/jmer.v3i2.1903

Table 1. The contribution of principal components to the yield of C element

No	Contribution	No	Contribution	No	Contribution
1	21.4085	7	5.175471	13	2.772642
2	12.38908	8	4.348705	14	1.887782
3	9.86408	9	4.101478	15	1.815436
4	7.824739	10	3.869279	16	1.592202
5	5.918989	11	3.355877	17	1.355792
6	5.646582	12	2.833679	18	1.254072

Table 2. The contribution of the main components to the yield of Mn element

No	Contribution	No	Contribution	No	Contribution
1	25.9899	6	6.124138	11	3.009176
2	12.78127	7	5.195127	12	2.801144
3	8.351011	8	4.785061	13	2.196297
4	8.048026	9	4.319319	14	1.763164
5	6.761434	10	3.676696	15	1.341023

Draw a histogram of the principal component contribution.

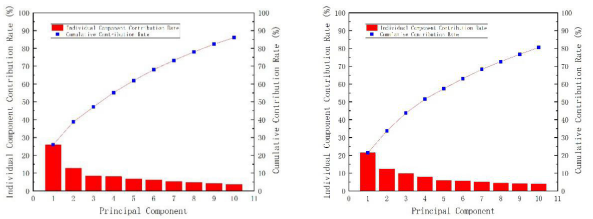

Figure 1. Cumulative contribution curve of each component to C and Mn yield

4.2 Multivariate Linear Analysis

Multiple regression analysis was realized, and the regression equation parameters as shown in Table 3 and Table 4 were obtained.

Table 3. Parameters of regression equation of C element

	Coefficients	Standard Error	t-Stat
Intercept	0.001047457	0.038356467	0.02730847
X Variable 1	0.031558432	0.017285959	1.82566858
X Variable 2	-0.090083783	0.022720995	-3.9647817
X Variable 3	-0.044355624	0.025666782	-1.7281334
X Variable 4	0.003899704	0.029307903	0.13305981
X Variable 5	-0.187262273	0.033143873	-5.6499817
X Variable 6	0.172774933	0.034694712	4.97986356
X Variable 7	0.141638615	0.035154676	4.02901213
X Variable 8	-0.008886455	0.038369742	-0.2316006
X Variable 9	0.194959025	0.039497437	4.93599184
X Variable 10	0.064962114	0.040714985	1.5955333

Table 4. Parameters of regression equation of Mn element

	Coefficients	Standard Error	t-Stat
Intercept	-0.000360189	0.05966	-0.00604
X Variable 1	-0.125833415	0.026164	-4.80947
X Variable 2	0.060258365	0.036076	1.670331
X Variable 3	-0.04655231	0.044574	-1.04438
X Variable 4	-0.004954195	0.046203	-0.10723
X Variable 5	-0.303739654	0.05332	-5.6965
X Variable 6	0.206682512	0.055104	3.750742
X Variable 7	0.037777314	0.058931	0.641044
X Variable 8	-0.171483094	0.061788	-2.77536
X Variable 9	-0.128368788	0.068568	-1.87214
X Variable 10	-0.052147585	0.070356	-0.74119

Knowing the regression parameters and the number of types of ingredients, a regression equation can be established to predict the yield of C and Mn elements online.

4.3 Linear Programming Results

For the convenience of calculation, the net weight of molten steel can be set to 70,000 kg. Establish a linear programming model and solve the cost-optimized batching plan. Related data is drawn into Table 5.

Table 5. Alloy batching plan (70,000kg molten steel)

Type	Inputs kg		
	HRB400	HRB500	Q345B
FeV55N11-A	5		6
Low Al ferrosilicon	2		4
Vanadium Nitrogen Alloy	4		2
FeV50-A	40		34
FeV50-B	0		0
Calcium Silicon Aluminum	75		24
FeAl30Si25	0		0
Silicon Aluminum Manganese Alloy Ball	10		6
Silicon Manganese Slag	34		36
FeSi75	2		4
FeSi75-B	3		0
Petroleum Coke Recarburizer	85		40
FeMn64Si27	1550		0
FeMn68Si18	0		1360
SiC(55%)	132		165
Silicon Calcium Carbon Deoxidizer	24		30

5. Conclusion

Based on principal component regression analysis and linear programming, optimizing the deoxidation alloying

DOI: https://doi.org/10.30564/jmer.v3i2.1903

batching plan is of great significance to actual production. The optimization model has universal significance and can be used in the production of any steel mill. When a large amount of process data is known, principal component regression analysis is used, and the main factors solved are used linear regression to obtain an optimized batching plan.

This optimization model is more directional and specific than regression analysis alone, and more general and applicable than linear programming alone. It can not only predict the yield of alloy elements online, but also obtain the optimization results of batching schemes, reduce costs, increase the yield of important elements, and improve the market competitiveness of steel mills; reduce the quality of scrap materials and play a positive role in ecological and environmental protection.

Reference

[1] Jingtao Hu. Development and online application of LF refining deoxidation alloying model[D]. Northeastern University, 2011.

[2] Chunxia Zhang. Deoxidation alloying control model of steelmaking process[A]. Chinese Metal Society. Proceedings of 1997 China Iron and Steel Annual Conference (Part 2)[C]. Chinese Metal Society: Chinese Metal Society, 1997: 4.

[3] Zhe Xu. Optimized setting and application of alloy addition amount in ladle refining furnace[D]. Shenyang: Northeastern University, 2019.

[4] Wenle Zhang. Research on alloying model of LF refining furnace[D]. Shenyang: Northeastern University, 2011.

[5] Ruonan Cheng, Ruimei Wang, Cong Ren, et al. Optimization of the "deoxidation alloying" batching scheme for molten steel[J]. Energy Saving, 2020, 39(02): 86-87.

[6] Yu Dai, Weiwei Xie, Jixiang Chen, et al. Analysis of deoxidation alloying ingredients based on gray correlation[J]. Scientific Consulting (Science and Technology Management), 2019(09): 31.

[7] Huiling Zhou, Qian Zhang, Xinyue Han, et al. Optimized design of deoxidation alloying scheme for converter smelting[J]. World Nonferrous Metals, 2019(13): 12-13.

[8] Fangyu Liu, Yi Zhou, Jiaxin Tang, et al. Optimization of the "deoxidation alloying" batching scheme for molten steel[J]. Modern Computer, 2019(22): 8-13.

[9] Pengmai Liu, Jiaming Zhu, Zhengshuai Gao, Yaning He. Analysis of deoxidizing alloying ingredients based on BP neural network[J]. Journal of Qilu University of Technology, 2019, 33(05): 74-80.

[10] Chunxia Zhang. Deoxidation alloying control model of steelmaking process[A]. Chinese Society of Metals. Proceedings of 1997 China Iron and Steel Annual Conference (Part 2)[C]. Chinese Metal Society: Chinese Metal Society, 1997: 4.

[11] Lei Li. Research on MES construction of metal smelting enterprises based on mass customization [D]. Ocean University of China, 2011.

[12] Jie Liu, Tao Wang. The application of multi-objective linear programming in the adjustment of product structure of iron and steel enterprises[J]. Theoretical Monthly, 2008(08): 171-173.

DOI: https://doi.org/10.30564/jmer.v3i2.1903

BILINGUAL PUBLISHING CO.
Pioneer of Global Academics Since 1984

Journal of Mechanical Engineering Research
http://ojs.bilpublishing.com/index.php/jmer

REVIEW

A Review on Utilization of Light Weight Fly Ash Cenosphere as Filler in both Polymer and Alloy-Based Composites

Shashikant Kushnoore[1*] Nitin Kamitkar[1] Vinay Atgur[1] Mallikarjun S Uppin[2] M. Satishkumar[3]

1. Koneru Lakshmaiah Educational Foundation, Guntur, Andhra Pradesh, India
2. Poojya Doddappa Appa College of Engineering, Kalaburagi, India
3. Qis College of Engineering and Technology, Ongole, Andhra Pradesh, India

ARTICLE INFO

Article history
Received: 5 March 2020
Accepted: 19 June 2020
Published Online: 24 June 2020

Keywords:
Fly ash cenosphere
Polymer and Alloy composites
Mechanical and Physical properties

ABSTRACT

Fly Ash Cenospheres (FACs) are obtained from the coal power plants in the form of hollow spherical particles by burning the coal. FAC was started to use in early 1980-1985 as lightweight filler material in producing composites of cementitious and at present many researchers are focusing on use of FAC as filler in polymer and metals. In this paper, the systematic review on research activities and application of FAC in manufacturing light weight products are done. The influence of FAC on the physical and mechanical properties of incorporated polymer and alloy-based composites were summarized. Prospects of future for its use were also suggested and summarized in this paper.

1. Introduction

The demand for high-performance materials in the latest technical materials is growing day by day. Composites are a mixture of two or more chemically distinct materials which will have improved properties over the individual materials [1]. These composites could be synthetic or natural and were flexible in nature because of their important properties like elevated high bending stiffness, modulus, chemical resistance and specific strength for multifunctional applications [2,3]. Combining two or more conventional materials can create new high-performance materials. In the current manufacturing industries hybrid materials play a significant role.

Engineering materials are mainly classified as metals and alloys, plastics, ceramics and glasses, and their combinations will form the evolution of composite materials as shown in Figure 1 [4]. The metal filled plastics in which plastic fibers are acting as reinforcement in metal matrix. In metal matrix composites various reinforcement materials were used like fly ash, cenosphere as ceramics. Where as in case of fiber reinforced plastics natural and synthetic fibers are used as reinforcement to get better properties plastic composites. Glass Reinforced Plastics (GRP), Carbon fiber reinforced polymer (CFRP), Polytetrafluoroethylene (PTFE) are various examples of combination of polymer with ceramics and glasses [5].

**Corresponding Author:*
Shashikant Kushnoore,
Koneru Lakshmaiah Educational Foundation, Guntur, Andhra Pradesh, India;
Email: shashikushnoore@gmail.com

 DOI: https://doi.org/10.30564/jmer.v3i2.1737

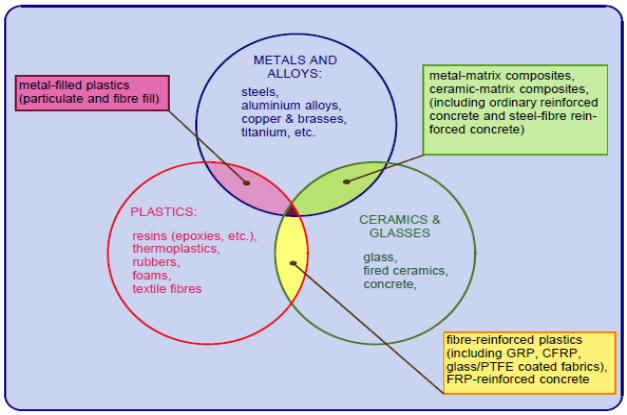

Figure 1. Classes of engineering materials, showing the evolution of composites

Two Greek words: Kenos (hollow, void) and Sphaera (sphere) coined the term Cenosphere. Cenosphere is a hollow ceramic microsphere contained in fly ash, as it is a natural by-product of coal combustion during electricity generation [6]. Cenosphere is recycled from the waste stream as a portion of the fly ash produced in coal combustion. They are consisting of alumina, inert silica, and iron. The cenosphere size ranges from 1 to 500 microns, with an average compressive capacity of 3000+psi. with a white and dark gray colour [7,9]. They are stated to as hollow spheres, microspheres, hollow ceramic microspheres, glass beads, or micro balloons.

The actual worldwide use of ash ranges greatly from a minimum of 3% to a maximum of 57%, but the global average is just 16% of total ash [8]. Throughout India as well as in many other countries, thermal power plants are the primary sources for power generation. India has about 40 major thermal power plants, and they have produced about two thirds of the country's power demands. India generates about 110 million tons of coal ash per year from the annual burning of about 300 million tons of coal for electricity generation. About 73 percent of India's total electricity generation capacity is thermal, 90 percent of it is based on coal [10].

1.1 Syntactic Foams

The synthetic foam concept was originally invented in 1955 by the Bakelite Company (New York) for its lightweight composites of hollow phenolic microspheres bonded to a phenolic, epoxy or polyester matrix [11]. Syntactic foams are examples of composite particulate materials consisting of hollow spherical fillers in a resin matrix [12]. Similar to solid particulate composites and fibre-reinforced composites, these hollow spheres are called micro ballons incorporated in the matrix. The Micro balloons have been used in syntactic foams, can be made of glass, ceramic, steel and aluminium available in different sizes [13,15].

These matrix materials have more influence on the tensile properties. The tensile strength could be enhanced by a chemical surface treatment of the particles, such as silanisation, which allows for the creation of strong bonds between glass particles and epoxy matrix. Including fibrous materials often improves tensile strength. Syntactic foams are typically structuring of two phases, namely matrix and micro-balloons. Due to the presence of porosity inside the micro-balloons these foams are known as closed porous foams. Nevertheless, air, or voids can be entrapped inside the matrix during the manufacture of syntactic foams. The presence of air or voids within the matrix is called open cell porosity and thus gives syntactic foams a three-phase structure [14].

The main contribution of syntactic foams to enhancing composite performance relies primarily on nature's buoyancy and insulation.

Buoyancy characteristics- including high strength, low density and low water absorption make the material suitable for applications with sub-surface buoyancy.

Current syntactic foam applications include the buoyancy modules for Remote operation of underwater vessels / Autonomous underwater exploration of underwater vessels / Ship hulls / Helicopter and aircraft parts.

Insulation characteristics - Syntactic foam has a low thermal conductivity coefficient which gives it superior properties, especially under highly compressive loads. It can be used for Liquefied Natural Gas (LNG) and industrial applications in underwater plumbing, load bearing insulation, subsea and insulation. The material's strength enables it to be used as a light weight, load carrying structure for marine, military and acoustic applications [16].

Many syntactic foam applications include: Deep-sea buoyancy foams, Thermoforming plug aids, Radar transparent materials, acoustically attenuating materials, Blast reducing materials, Sports goods such as tennis rackets and soccer balls, Drilling devices, Riser buoyancy, Upstream SURF ancillary gear, Mooring buoyancy, Deepwater buoyancy, Subsea buoyancy, Defense / oceanographic buoyancy.

1.2 Cenosphere

The cenosphere (spherical shape) improves the flow capacity in most applications and provides an even distribution of the composite matrix filler material. Cenospheres are 75 percent lighter than other commonly used minerals as fillers or extender. It is possible to use them in dry or wet slurry form due to the natural properties of the cenosphere [17]. Cenosphere is easy to manage because of its

DOI: https://doi.org/10.30564/jmer.v3i2.1737

inert properties and has a low surface area-to-volume ratio and is not influenced by liquids, solvents, alkalis or acids etc.

These hollow spheres used as an extender for plastic compounds and are compatible with thermoplastics, latex, polyesters, plastisol's, epoxies, phenolic resins and urethanes [18]. Synthetic cenosphere foams have shown superior mechanical properties compared to those fabricated with microspheres [19]. Due to lower production costs of cenospheres often replace mined materials. the cenosphere will support the finished product properties by increasing electrical insulation, durability and better sound proofing [18]. Cenosphere compatibility, especially in cements and other building materials, such as wall coatings and composites, and also used in a wide range of other items, including sports equipment, insulation, vehicles, marine crafts, paints, and fire and heat protection devices [20].

Currently, the manufacturers have begun filling the cenospheres in metals and polymers in order to make light-weight composite materials with higher strength, when compared with the other types of foam materials.

Table.1 Chemical composition of fly ash cenosphere

Sl.No	Element	% of composition
1	Silicon Oxide (Sio_2)	93.28
2	Aluminium Oxide (Al_2O_3)	0.33
3	Ferric Oxide (Fe_2O_3)	0.57
4	Calcium Oxide (CaO)	0.63
5	Loss On Ignition	4.80
6	Magnesium Oxide (MgO)	0.34

2. Literature Review

A few inquiries were recorded concerning the physical and mechanical properties of polymer and alloy composites reinforced by fly ash cenosphere.

2.1 Cenosphere Reinforced Polymer Composites

Das A and Satapathy BK [21] prepared composite by adding cenosphere and Polypropylene and to study their structural and mechanical properties such as flexural and tensile. Morphological properties of the composite were studied using Wide-angle X-ray diffraction (WAXD) and scanning electron microscopy and they found that increase in tensile and flexural properties increased with 30% of reinforcement.

Labella M et al [22] prepared the composite by adding Vinyl ester filled with fly ash cenospheres. By adding the cenosphere the flexural strength decreased by 73% while the flexural modulus increased by 47% at 60 vol. % cenospheres. They also found that coefficient of thermal expansion decrease by reinforcing the composite with the cenosphere.

Chand N et al [23] studied how cenosphere could be used as a filler to improve the mechanical properties of the polymer matrices. Due to the homogeneous dispersion of cenospheres in polymer matrix it also exhibits improved wear resistance of high density poly ethylene composites.

Takuya Morimoto et al [24] have investigated porous particles filled phenolic composites. They found that the fracture toughness and the wear rate decreased as the volume fraction of hollow particles increased.

Gupta N et al [25] have done the work on syntactic foams. The mechanical properties and density of the syntactic foam could be changed by using different inner radius but cenospheres of same outer radius in the matrix.

Chauhan SR and Thakur S [26] were prepared the specimens with varying particle size cenosphere reinforced vinyl ester composite It was found that cenosphere particles of submicron size as fillers contributed to the improvement of the specific wear rate and the mechanical properties significantly, for all the vinyl ester composites it decreases with sliding distance and after certain duration attains approximately a steady state value.

Sampathkumaran P et al [27] have carried work on fly ash cenosphere reinforced different polymer composites, and they found that improved properties of both physical and mechanical properties with respect high density poly ethylene (HDPE) and low density poly ethylene (LDPE) polymer composites.

Divya VC et al [28] have carried out work on the composite, with a high density polyethylene, cenosphere and multiwall carbon nanotubes (MWCNT), and they found that these composites showed better mechanical properties than the composites without cenosphere and MWCNT. The addition of cenosphere and MWCNT increase the flammability property of the composite.

Jalageri HB et al [29] have prepared the cenosphere/multi wall carbon nano tubes reinforced polymer composites, and they found that the composite with 0.5 wt. % exhibits higher impact strength, and for 0.1 to 0.2 wt. % of MWCNT were found good flexural and tensile properties.

Ren S et al [30] were demonstrated that Fly ash Cenospheres-hollow glass microspheres / borosilicate glass composites (FACs-HGMs / BG) have outstanding mechanical properties both at room and high temperatures can be used in the near future as potential candidates for structural materials or temperature-resistant buoyant material.

Balaji R et al [31] prepared phenolic composites filled with Cenosphere, and studied their thermo-oxidation,

 DOI: https://doi.org/10.30564/jmer.v3i2.1737

properties and its characteristics. They found that decrease in the thermal degradation occurred due to composite filled with the cenosphere.

Wang MR et al [32] prepared the geopolymeric based composites by adding metakaolin and fly ash cenosphere based geopolymeric slurry. They found that by the transmission electron microscopy and scanning electron microscope in alkaline condition fly ash cenosphere did not dissolve. 40 vol. % of this composite gives promising material for intermediate-temperature thermal insulation.

Bora PJ et al [33] were prepared the composites by solution-processing of Polyvinylbutyral (PVB)-FAC, PVB-CoOx-FAC and PVB-NiO-FAC. Such composites are suitable for applications focused on microwave absorption such as robotic engineering, radar, electromagnetic gasket, military, aircraft and unmanned vehicles.

Balaji R and Sasikumar M [34] were prepared the composite of cenosphere filled phenolic of ceramic woven. The oxyacetylene ablation test and Thermogravimetric Analysis were used to study the ablative properties and thermal properties. They found that thermal degradation of cenosphere filled composites increases with the increase in concentration of cenosphere.

Sambyal P et al [35] have studied the advanced poly (aniline-co-toluidine)/flyash corrosion resistance properties on mild steel substrates using powder coating techniques, and noble potential for epoxy with copolymer-coated steel coated specimens relative to epoxy-coated steel. They noticed even low corrosion current for 2.0 and 3.0 wt coatings. Copolymer composite loading per cent at 3.5 wt. % NaCl solution.

Sharma J et al [36] have carried out work on effect of fly ash cenosphere on dielectric properties of low-density polyethylene (LDPE) and found that the variation of the relative dielectric constant with frequency indicates the presence of material interface polarization processes at low frequency. They also found that there is little variance in alternative current conductivity with rising cenosphere concentration.

GU J et al [37] characterize filler/matrix and hollow structure characteristic (porosity). They have investigated damping properties of the composites in the temperature range of 40 to 150 0C and they found better damping properties than matrix.

Angadi SB et al [38] have prepared epoxy composite reinforced with cenosphere. They have carried out experimental investigation on drilling characteristics of prepared composite. They have considered drilling aspects, such as hole, thrust and drilled hole surface roughness. They have prepared specimens at different wt. % of cenosphere in epoxy resin as the composite matrix, and found that the reduced thrust forces of lower diameter drill bit, whereas greater surface roughness were found for lower diameter drilled hole. Cenosphere addition of 60% shows a significant reduction in surface roughness and thrust force.

2.2 Cenosphere Reinforced Alloy Composites

Chandel V et al [39] Identified potential applications of Al 7075 alloy as matrix and cenosphere as reinforcement in the aircraft and space industries due to lower weight to strength ratio, creep resistance and high wear resistance. They suggested that composites are likely to overcome the cost barrier as well as the various physical and mechanical properties for use worldwide today and serve a wide range of applications.

Vikrant C and Onkar SB [40] found that cenosphere as reinforcement in Al 7075 alloy as matrix have been used widely in various applications because of their lower weight to strength ratio, wear resistance and creep resistance such as aircraft and space industries.

Goel MD et al [41] studied the compressive deformation by varying densities and cenosphere sizes at different strain rates (from 0.01/s to 10/s) of aluminum cenosphere syntactic foams. It was found that relative density will not affect the densification strain, strain rate and cenosphere size. But, relative density and cenosphere size affect the plateau stress and energy absorption of syntactic foams.

Birla S et al [42] using casting technique and CaH2 as a foaming agent prepared the Al-Si-Cu-Mg-cenosphere hybrid foams (HFs) of varying relative densities. They have found that the addition of cenospheres up to 30 vol. % improved the yield strength, plastic collapse stress, and plateau stress. Hybrid foam energy absorption is increasing with cenosphere size decrease and relative density increase. It was also discovered that densification strain is almost invariant with cenosphere size.

Rohatgi PK et al [43] studied the mechanical behavior and microstructure f die casting AZ91D magnesium alloy -fly ash cenosphere composites. The presence of fly ash cenospheres in AZ91D has been reported to result in significant refinement of the surrounding matrix alloy, which becomes more intense with the increasing weight percentage of fly ash. They also investigated that the hardness of the composites based on AZ91D was improved by the introduction of fly ash, the composite toughness was a maximum where 5 wt. % fly ash was added and becomes slightly lower with the addition of 10 and 15 wt. % fly ash.

Kumarasamy SP et al [44] carried out work on the Hybrid Aluminum Metal Matrix Composites (HAMMC) by reinforcing constant quantities of fly ash cenosphere (10%) and varying quantities of graphite (2%, 4% and 6%),

DOI: https://doi.org/10.30564/jmer.v3i2.1737

cenosphere, hardness and tensile strength were found to increase and vice versa for graphite addition. Owing to reinforcement particles, the improved tensile strength of the Aluminum matrix from 178 N/mm^2 to 213 N/mm^2 as for the composite is concerned. The wear resistance improves considerably with the addition of cenosphere and but there is a wear rate decreases with graphite addition due to its self-lubricating nature. They found that minimizing the surface roughness of developed composite, the cutting speed and % of graphite addition have the major contribution.

Huang Z and Yu S [45] were carried out work on 5 wt. % and 100 microns of fly ash cenosphere particles integrated in the AZ91DMg alloy to manufacture in situ Mg2Si and MgO strengthened AZ91D / Flyash composites using compo casting technique. They observed that the cenosphere particles were distributed homogenously in the alloy matrix, and filled with the alloy matrix on most of the cenosphere particles.

Vishwakarma A et al [46] carried out the study on analysis of various cenosphere sizes at different applied pressures and sliding speeds for dry sliding aluminum alloy (LM13) cenosphere syntactic foam behaviour. They have found that the coefficient of friction, frictional heating and the wear rate decreases with the decrease in cenosphere depth. They also found that the yield strength of syntactic foam increases with the decrease in cenosphere size, the wear rate also decreases with the decrease in cenosphere size and the increased strength often leads to increased wear resistance by decreasing the size of the cenosphere.

Uju WA and Oguocha INA [47] prepared the composite of Al-Mg alloy A535 reinforced with a mixture of 5 wt. % silicon carbide and 5 wt. % fly ash with varying wt. % fly ash particles. They found that by adding fly ash and silicon carbide, the coefficient of thermal expansion of A535 goes on decreasing.

Saravanan V et al [48] found that 10 vol. Cenosphere percent reinforced aluminum alloy (AA) 6063 composite as the most suitable material for brake disks instead of more costly particles of aluminum oxide (Al_2O_3) or silicon carbide (SiC).

Luong DD et al [49] found that energy-absorption potential of A4032 / fly ash cenosphere composites were higher at higher strain levels.

3. Conclusion

The role of density, hardness, wear resistance, co-efficient of friction, slide wear and strength properties of cenosphere reinforced polymers and alloy composites were clearly identified and summarized.

The density value drops when the thermoplastic polymers is filled in with the fly ash cenospheres. With the addition of cenosphere filler, the hardness value of thermoplastic polymers had improved. With the introduction of FAC fillers, the compression and impact strengths decrease, and the variance in the compression strength value was least for LDPE.

It was found that slide wear resistance of cenosphere filled composites showed better results when compared with the un-filled composites. Further, the wear loss also increases with the increase in load of both un-filled and filled composite specimens.

Cenosphere reinforced polymer samples coefficient of friction values were slightly lower than those of unfilled counterparts. Filling cenospheres in polymer and alloys has made a significant contribution to reducing friction, and increases wear resistance.

The investigation of the polymer materials has been confirmed as the best option for wear resistance applications, particularly HDPE. Owing to its improved slide wear properties, lower friction coefficient, lower percentage reduction in compression strength and impact energy compared to other polymer materials.

It was observed that with the addition of weight percentage of fly ash in both the polymer and alloy composites, there was an improvement in tensile strength, compressive strength as well as hardness. Whereas in the case of both polymer and alloy composites the ductility decreases with the percentage weight percentage of fly ash. It is also concluded that with an increase in particle size of fly ash cenosphere reinforced alloy composites the tensile strength, compressive strength & hardness decreases.

In case of alloy composites, it was found that fly ash cenosphere was mainly added in aluminium alloy when compared with the other alloys. FAC reinforced alloy composites have shown a vital applications in the aerospace industries because of their light weight, high tensile strength and hardness.

As fly ash cenosphere is made with hollow spheres, it was observed that the distribution of FAC at molecular level in polymer and alloy composites matrix were not much uniform and also the chances of getting blow holes due to its porous nature. To overcome this problem and getting the newer techniques for the preparation of FAC composites, becomes challengeable in the current scenario.

From the above literature review, it has been concluded that the fly ash cenosphere reinforced polymer and alloy composites had played an important role in the structural applications, aerospace industries and naval applications because of their light weight, wear resistant, anti-corrosion

 DOI: https://doi.org/10.30564/jmer.v3i2.1737

and buoyancy in nature. In the current scenario the production of composites with low environmental impact and strong commercial viability has become a big trend. Thus, the use of FAC in polymer and metal matrix composites also plays an significant role in greenhouse emissions by avoiding the other widely used mineral fillers.

References

[1] ASM International Engineered Materials Handbook, Desk Edition, 1995. www.asm-intl.org

[2] L Mohammed , M N M Ansari, G Pua, J Mohammad, IM Saiful. A Review on Natural Fiber Reinforced Polymer Composite and Its Applications. International Journal of Polymer Science, 2015.

[3] KY Lee, A Yvonne , AB Lars, O Kristiina, B Alexander. On the use of nanocellulose as reinforcement in polymer matrix composites. Composites Science and Technology, 2014, 105: 15-27.

[4] Bryan Harris Engineering composite materials. The Institute of Materials, London, 1999.

[5] PH Holloway, P N Vaidyanathan. Characterization of Metals and Alloys. Momentum Press, New York, 1993.

[6] K Friedrich, S Fakirov, Z Zhang. Polymer Composites: From Nano- to Macro-Scale. Springer, America, 2005.

[7] Parker Jacob. Fly Ash: Properties, Analysis and Performance. Nova Science Publishers, UK 2017.

[8] S Firat, G S Yılmaz, T Comert, M Sumer. Utilization of marble dust, fly ash and waste sand (Silt-Quartz) in road subbase filling materials. KSCE Journal of Civil Engineering, 2012: 16(7).

[9] BI Oza, A S Amin. Effect of untreated Cenosphere on Mechanical properties of Nylon-6. International Journal on Recent and Innovation Trends in Computing and Communication, 2015, 3(2321-8169).

[10] S Anandhan. Recent Trends in Fly Ash Utilization in Polymer Composites. Int J Waste Resources, 2014, 4(3).

[11] Syntactic Foam Oxford English Dictionary citation of science: News Let. 2 Apr. 213/3.

[12] ASTM International. Engineering Materials Handbook. , 1995. www.astm.org

[13] A H Landrock. Handbook of Plastic Foams: Types, Properties, Manufacture and Applications. Edited Noyes Publications, New Jersey, 1995, 147-163.

[14] J Rahul, T Hareesh. Processing, compression response and finite element modeling of syntactic foam based interpenetrating phase composite (IPC). Materials Science and Engineering A, 2009, 499: 507-517.

[15] N Gupta, B S Brar, B S Woldesenbet. Effect of filler Addition on the Compressive and Impact Properties of Glass Fibre Reinforced Epoxy. Bulletin of Materials Science, 2001, 2: 219-223.

[16] K V Joseph, F Finjin, C Joyson, P Das, G Hebbar. FLY Ash Cenosphere Waste Formation in Coal Fired Power Plants And Its Application as A Structural Material - A Review, International Journal of Engineering Research & Technology, 2013, 2(8).

[17] N Ranjbar, C Kunzel. Cenospheres: A review. Fuel, 2017, 207: 1-12.

[18] B R Manjunath, P Sadasivamurthy, P V Reddy, R H Karickal. Studies on cenosphere as fillers for PVC compounds for application in electrical cables. Journal of the American Institute of Chemists Volume, 2013, 86(1).

[19] K R Pradeep, G Nikhil, F S Benjamin, D L Dung. The synthesis, compressive properties, and applications of metal matrix syntactic foams. The Journal of the Minerals, Metals & Materials Society, 2011, 63(2): 36-42.

[20] Johann Thim. Performing plastics - How plastics set out to conquer the world of sports. European Chemical Industry Council 2005, Retrieved 2009-08-07.

[21] A Das, B K Satapathy. Structural, thermal, mechanical and dynamic mechanical properties of cenosphere filled polypropylene composites. Materials and Design, 2011, 32: 1477-1484.

[22] M Labella, E S Zeltmann, V C Shunmugasamy, N Gupta, R K Pradeep. Mechanical and thermal properties of fly ash/vinyl ester syntactic foams. Fuel, 2014, 121: 240-249.

[23] N Chand, P Sharma, M Fahim. Correlation of mechanical and tribological properties of organosilane modified cenosphere filled high density polyethylene. Materials Science and Engineering A, 2010, 527: 5873-5878.

[24] T Morimoto, T Suzuki, H Iizuka. Wear rate and fracture toughness of porous particle-filled phenol composites. Composites Part B, 2015, 77: 19-26.

[25] N Guptaa, E Woldesenbet, P Mensah. Compression properties of syntactic foams: effect of cenosphere radius ratio and specimen aspect ratio. Composites: Part A, 2004, 35: 103-111.

[26] S R Chauhan, S Thakur. Effects of particle size, particle loading and sliding distance on the friction and wear properties of cenosphere particulate filled vinylester composites. Materials and Design, 2013, 51: 398-408.

[27] P Sampathkumaran, Kishore, S Seetharamu, V V Pattanashetti, V V Kumar, S M Kumar, H B Niranjan. Fly ash cenospheres as reinforcement in different polymer composites - a comparative study of physi-

DOI: https://doi.org/10.30564/jmer.v3i2.1737

cal and mechanical properties. Indian Journal of Engineering & Material Sciences, 2015, 22: 354-362.

[28] V C Divya, M K Ameen, R B Nageshwar, R R Sailaja. High density polyethylene / cenosphere composites reinforced with multi-walled carbon nanotubes: Mechanical, thermal and fire retardancy studies. Materials and Design, 2015, 65: 377-386.

[29] H B Jalageri, G U Raju, K G Kodancha. Experimental Investigations on Mechanical Properties of Cenosphere/MWCNT Reinforced Polymer Nanocomposites. American Journal of Materials Science, 2015, 5(3C): 101-106.

[30] S Ren, X Tao, X Ma, J Liu. Fabrication of fly ash cenospheres-hollow glass microspheres/borosilicate glass composites for high temperature application. Ceramics International, 2017, 44(1).

[31] R Balaji, M Sasikumar, A Elayaperumal. Thermal, thermo oxidative and ablative behavior of cenosphere filled ceramic/phenolic composites. Polymer Degradation and Stability, 2015, 114: 125-132.

[32] M R Wang, D C Jia, P G He, Yu Zhou. Microstructural and mechanical characterization of fly ash cenosphere/metakaolin-based geopolymeric composites. Ceramics International, 2011, 37: 1661-1666.

[33] P J Bora, M Porwal, K J Vinoy, Kishore, P C Ramamurthy, M Giridhar. Industrial waste fly ash cenosphere composites based broad band microwave absorber. Composites Part B: Engineering, 2018, 134(1): 151-163.

[34] R Balaji, M Sasikumar. A study on the effect of cenosphere on thermal and ablative behavior of cenosphere loaded ceramic/phenolic composites. Polymer, 2014, 55: 6634-6639.

[35] P Sambyal, G Ruhi, Bhandari Hema, K D Sundeep. Advanced anti corrosive properties of poly (aniline-co-o-toluidine)/ flyash composite coatings. Surface & Coatings Technology, 272: 129-140, 2015.

[36] J Sharma, N Chand, M N Bapat. Effect of cenosphere on dielectric properties of low density polyethylene. Results in Physics, 2012, 2: 26-33.

[37] J Gu, G Wu, X Zhao. Damping properties of fly ash/ epoxy composites. Journal of University of Science and Technology Beijing, 2008, 15(4): 509.

[38] S B Angadi, R Melinamani, V Gaitonde, M Doddamani, S R Karnik. Experimental Investigations on Drilling Characteristics of Cenosphere Reinforced Epoxy Composites. Applied Mechanics and Materials, 2015, 766-767: 801-811.

[39] V Chandel, O S Bhatia, M S Sethi. Fabrication and Characterization of Al 7075-Cenosphere Composite & Its Comparison with Pure Al 7075: A Review. International Journal of Research Studies in Science, Engineering and Technology, 2015, 2(3): 7-20.

[40] C Vikrant and S B Onkar. Fabrication and Characterization of Al 7075-Cenosphere Composite & its comparison with pure Al 7075. International Journal of Engineering Trends and Technology, 2015, 29(3).

[41] M D Goel, D P Mondal, M S Yadav, S K Gupta. Effect of strain rate and relative density on compressive deformation behavior of aluminum cenosphere syntactic foam. Materials Science & Engineering A, 2014, 590: 406-415.

[42] S Birla, D P Mondal, S Das, D K Kashyap. Effect of cenosphere content on the compressive deformation behaviour of aluminum-cenosphere hybrid foam. Materials Science & Engineering A, 2017, 685: 213-226.

[43] P K Rohatgi, A Daoud, B F Schultz, T Puri. Microstructure and mechanical behavior of die casting AZ91D-Fly ash cenosphere composites. Composites: Part A, 2009, 40: 883-896.

[44] S P Kumarasamy, Vijayananth Kavimani, T Thankachan, G P Muthukutti. Investigations on mechanical and machinability behavior of aluminum/ flyash cenosphere /Gr hybrid composites processed through compocasting. Journal of Applied Research and Technology, 2017, 15(5): 430-441.

[45] Z Huang, S Yu. Microstructure characterization on the formation of in situ Mg2Si and MgO reinforcements in AZ91D/Flyash composites. Journal of Alloys and Compounds, 2011, 509: 311-315.

[46] A Vishwakarma, D P Mondal, S Birla, S Das. Effect of cenosphere size on the dry sliding wear behaviour LM13- cenosphere syntactic foam. Tribology International, 2017, 110: 8-22.

[47] W A Uju, I N Oguocha. A study of thermal expansion of Al-Mg alloy composites containing fly ash. Materials and Design, 2012, 33: 503-509.

[48] V Saravanan, P R Thyla, S R Balakrishnan. A low cost, light weight cenosphere-aluminium composite for brake disc application. Bull. Mater. Sci., 2016, 39 (1): 299-305.

[49] D D Luong, N Gupta, A Daoud, P K Rohatgi. High strain rate compressive characterization of aluminum alloy/ Fly ash cenosphere composites. JOM, 2011, 63(2).

 DOI: https://doi.org/10.30564/jmer.v3i2.1737

Author Guidelines

This document provides some guidelines to authors for submission in order to work towards a seamless submission process. While complete adherence to the following guidelines is not enforced, authors should note that following through with the guidelines will be helpful in expediting the copyediting and proofreading processes, and allow for improved readability during the review process.

Ⅰ. Format

- Program: Microsoft Word (preferred)
- Font: Times New Roman
- Size: 12
- Style: Normal
- Paragraph: Justified
- Required Documents

Ⅱ. Cover Letter

All articles should include a cover letter as a separate document.

The cover letter should include:

- Names and affiliation of author(s)

The corresponding author should be identified.

Eg. Department, University, Province/City/State, Postal Code, Country

- A brief description of the novelty and importance of the findings detailed in the paper

Declaration

v Conflict of Interest

Examples of conflicts of interest include (but are not limited to):

- Research grants
- Honoria
- Employment or consultation
- Project sponsors
- Author’s position on advisory boards or board of directors/management relationships
- Multiple affiliation
- Other financial relationships/support
- Informed Consent

This section confirms that written consent was obtained from all participants prior to the study.

- Ethical Approval

Eg. The paper received the ethical approval of XXX Ethics Committee.

- Trial Registration

Eg. Name of Trial Registry: Trial Registration Number

- Contributorship

The role(s) that each author undertook should be reflected in this section. This section affirms that each credited author has had a significant contribution to the article.

1. Main Manuscript
2. Reference List
3. Supplementary Data/Information

Supplementary figures, small tables, text etc.

As supplementary data/information is not copyedited/proofread, kindly ensure that the section is free from errors, and is presented clearly.

Ⅲ. Abstract

A general introduction to the research topic of the paper should be provided, along with a brief summary of its main results and implications. Kindly ensure the abstract is self-contained and remains readable to a wider audience. The abstract should also be kept to a maximum of 200 words.

Authors should also include 5-8 keywords after the abstract, separated by a semi-colon, avoiding the words already used in the title of the article.

Abstract and keywords should be reflected as font size 14.

Ⅳ. Title

The title should not exceed 50 words. Authors are encouraged to keep their titles succinct and relevant.

Titles should be reflected as font size 26, and in bold type.

Ⅳ. Section Headings

Section headings, sub-headings, and sub-subheadings should be differentiated by font size.

Section Headings: Font size 22, bold type

Sub-Headings: Font size 16, bold type

Sub-Subheadings: Font size 14, bold type

Main Manuscript Outline

Ⅴ. Introduction

The introduction should highlight the significance of the research conducted, in particular, in relation to current state of research in the field. A clear research objective should be conveyed within a single sentence.

Ⅵ. Methodology/Methods

In this section, the methods used to obtain the results in the paper should be clearly elucidated. This allows readers to be able to replicate the study in the future. Authors should ensure that any references made to other research or experiments should be clearly cited.

Ⅶ. Results

In this section, the results of experiments conducted should be detailed. The results should not be discussed at length in

this section. Alternatively, Results and Discussion can also be combined to a single section.

Ⅷ. Discussion

In this section, the results of the experiments conducted can be discussed in detail. Authors should discuss the direct and indirect implications of their findings, and also discuss if the results obtain reflect the current state of research in the field. Applications for the research should be discussed in this section. Suggestions for future research can also be discussed in this section.

Ⅸ. Conclusion

This section offers closure for the paper. An effective conclusion will need to sum up the principal findings of the papers, and its implications for further research.

Ⅹ. References

References should be included as a separate page from the main manuscript. For parts of the manuscript that have referenced a particular source, a superscript (ie. [x]) should be included next to the referenced text.

[x] refers to the allocated number of the source under the Reference List (eg. [1], [2], [3])

In the References section, the corresponding source should be referenced as:

[x] Author(s). Article Title [Publication Type]. Journal Name, Vol. No., Issue No.: Page numbers. (DOI number)

Ⅺ. Glossary of Publication Type

J = Journal/Magazine

M = Monograph/Book

C = (Article) Collection

D = Dissertation/Thesis

P = Patent

S = Standards

N = Newspapers

R = Reports

Kindly note that the order of appearance of the referenced source should follow its order of appearance in the main manuscript.

Graphs, Figures, Tables, and Equations

Graphs, figures and tables should be labelled closely below it and aligned to the center. Each data presentation type should be labelled as Graph, Figure, or Table, and its sequence should be in running order, separate from each other.

Equations should be aligned to the left, and numbered with in running order with its number in parenthesis (aligned right).

Ⅻ. Others

Conflicts of interest, acknowledgements, and publication ethics should also be declared in the final version of the manuscript. Instructions have been provided as its counterpart under Cover Letter.

About the Publisher

Bilingual Publishing Co. (BPC) is an international publisher of online, open access and scholarly peer-reviewed journals covering a wide range of academic disciplines including science, technology, medicine, engineering,education and social science. Reflecting the latest research from a broad sweep of subjects, our content is accessible worldwide – both in print and online.

BPC aims to provide an analytics as well as platform for information exchange and discussion that help organizations and professionals in advancing society for the betterment of mankind. BPC hopes to be indexed by well-known databases in order to expand its reach to the science community, and eventually grow to be a reputable publisher recognized by scholars and researchers around the world.

BPC adopts the Open Journal Systems, see on http://ojs.s-p.sg

Database Inclusion

Asia & Pacific Science Citation Index

Creative Commons

China National Knowledge Infrastructure

Google Scholar

Crossref

MyScienceWork

BILINGUAL
PUBLISHING CO.
Pioneer of Global Academics Since 1984

Tel:+65 65881289
E-mail:contact@bilpublishing.com
Website:www.bilpublishing.com

ISSN 2630-4945
02